THE JOURNAL OF PHYSICAL CHEMISTRY LETTERS
A JOURNAL OF THE AMERICAN CHEMICAL SOCIETY

pubs.acs.org/JPCL

Letter

Curvature of the Retroviral Capsid Assembly Is Modulated by a Molecular Switch

Tyrone Thames,[#] Alexander J. Bryer,[#] Xin Qiao,[#] Jaekyun Jeon, Ryan Weed, Kaylie Janicki, Bingwen Hu, Peter L. Gor'kov, Ivan Hung, Zhehong Gan, Juan R. Perilla,* and Bo Chen*

Cite This: *J. Phys. Chem. Lett.* 2021, 12, 7768–7776

Read Online

ACCESS | Metrics & More | Article Recommendations | Supporting Information

ABSTRACT: During the maturation step, the retroviral capsid proteins (CAs) assemble into polymorphic capsids. Their acute curvature is largely determined by 12 pentamers inserted into the hexameric lattice. However, how the CA switches its conformation to control assembly curvature remains unclear. We report the high-resolution structural model of the Rous sarcoma virus (RSV) CA $T = 1$ capsid, established by molecular dynamics simulations combining solid-state NMR and prior cryoelectron tomography restraints. Comparing this with our previous model of the RSV CA tubular assembly, we identify the key residues for dictating the incorporation of acute curvatures. These residues undergo large torsion angle changes, resulting in a 34° rotation of the C-terminal domain relative to its N-terminal domain around the flexible interdomain linker, without substantial changes of either the conformation of individual domains or the assembly contact interfaces. This knowledge provides new insights to help decipher the mechanism of the retroviral capsid assembly.

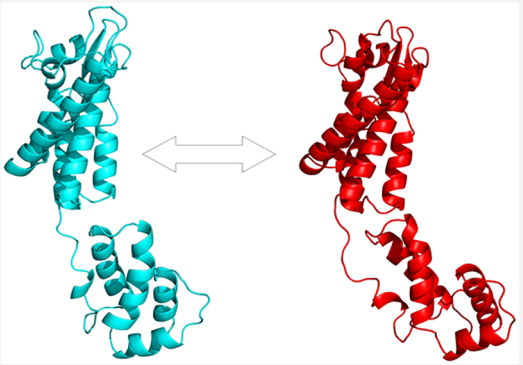

A mature retroviral capsid is assembled with more than 1000 copies of the capsid protein (CA) during a process in the virus life cycle called "maturation", which finalizes the capsid structure.[1] Despite limited sequence similarity, monomeric orthoretroviral CAs share a nearly identical three-dimensional fold.[2] Briefly, a CA contains two independently folded domains joined by a short flexible linker,[3] with the N-terminal domain (NTD) comprising a short β-hairpin followed by seven α-helices,[4,5] and the C-terminal domain (CTD) consisting of a short 3_{10} helix followed by four additional α-helices.[6] Intriguingly, these CAs form polymorphic capsids of distinct morphologies for different viruses, including tubular, polyhedral, and conical structures.[2,7] It has been shown that proper capsid assembly is critical for viral propagation and infectivity.[1,8] Thus, CAs and their assemblies are promising antiviral drug targets.[9,10] However, because of the strong polymorphism,[2,11] the detailed molecular basis of retroviral capsid assembly remains elusive.

Analyses of *in vivo* and *in vitro* assemblies have proven that the polymorphism and particular shapes of retroviral capsids are determined by insertion of 12 CA pentamers at varying locations in the hexameric lattice.[7,12] By now, a great deal has been learned about various retroviral CA hexameric assemblies by studying *in vitro* assemblies.[11] They were found to be stabilized by four intermolecular interfaces;[13−16] individual subunits within each hexamer are held together by the NTD−NTD interface between the first three helices, with corresponding CTDs tethered to the NTD via the NTD-CTD interface between helixes 4 and 8. Then, adjacent hexamers are bound together by the CTD dimer interface across helix 9 and the CTD trimer interface between helixes 10 and 11. Similar interfaces were observed in the Rous sarcoma virus (RSV) CA $T = 1$, 3 capsids and its hexameric assemblies,[17−20] which demonstrates that different retroviruses adopt a common hexameric and even pentameric assembly motif and suggests that potentially they employ a similar curvature control mechanism.

A key unresolved question is the mechanism of the curvature management in the retroviral capsid assembly. At the site-specific molecular level, little is known about how the CA modulates its conformation to switch between the pentameric and hexameric state and how it rearranges to accommodate the curvature variation in the pure hexameric lattice. When comparing isolated pentamers formed by cross-linked CAs and their counterpart hexamers,[21] CTDs were found to exhibit a variety of orientations. This agrees with atomic resolution models of different shaped mature HIV capsids constructed by molecular dynamics (MD) simulations.[16] However, these cross-linked oligomers are in an isolated state with disrupted CTD dimer and trimer interfaces. Moreover, cryoelectron tomog-

Received: June 4, 2021
Accepted: August 2, 2021
Published: August 10, 2021

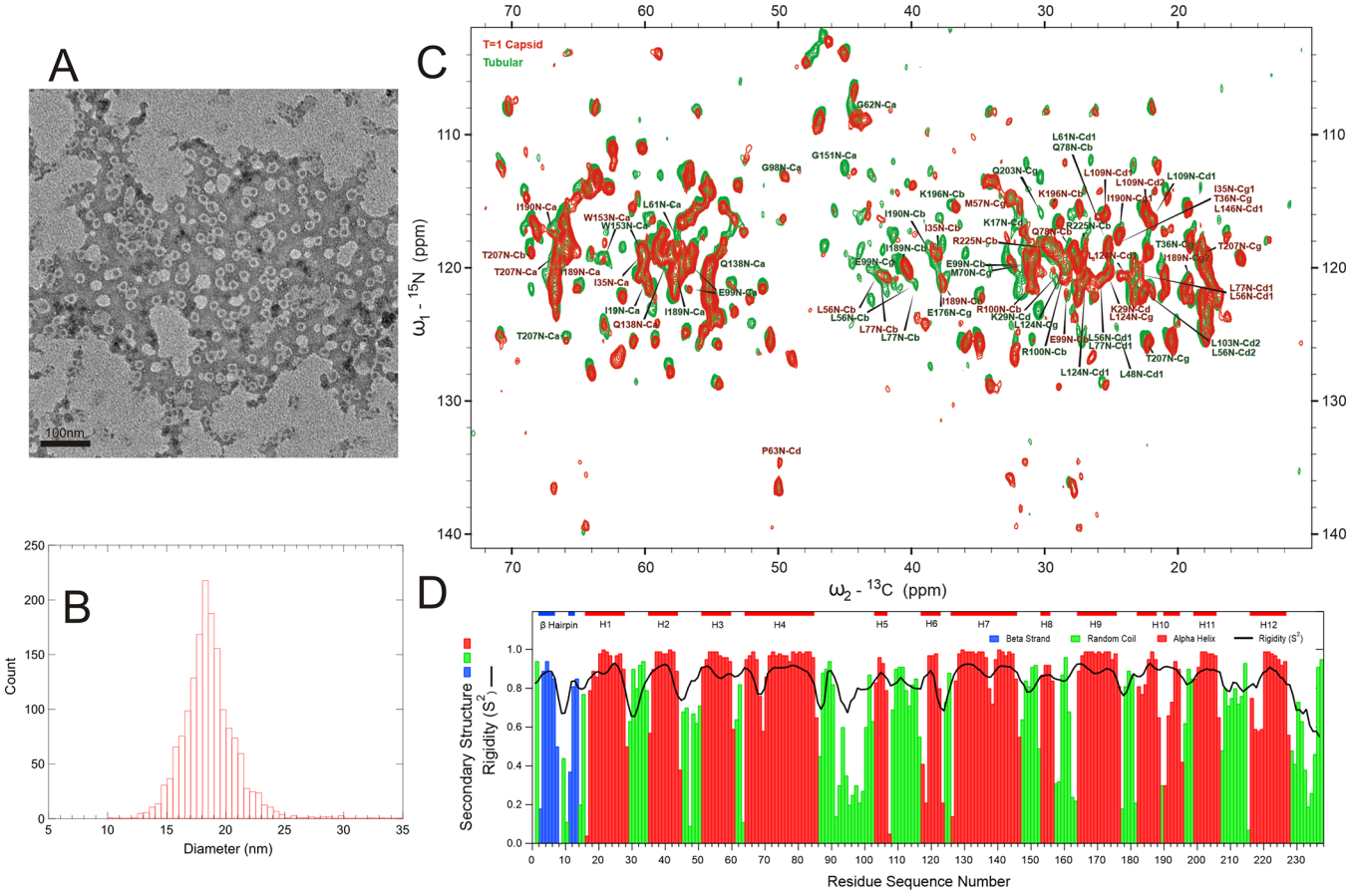

Figure 1. TEM and ssNMR characterization of the RSV CA $T = 1$ capsid assembly. (A) Negatively stained TEM image of the RSV CA I190V $T = 1$ capsid assembly. The operating magnification is 25 000-fold. (B) The average diameter of observed assemblies is ~18.5 nm as shown by the histogram. (C) 2D $^{15}N-^{13}C$ correlation spectra overlay of the $T = 1$ capsid assembly by the RSV I190V CA (red, this work) and the tubular assembly by the wild-type RSV CA (green).[33] For clarity, only those residues showing a change of either ^{13}C or ^{15}N resonances ≥2.0 ppm are labeled, red for the $T = 1$ capsid and green for the tubular assembly, respectively. (D) Site-specific prediction of the secondary structure and rigidity by TALOS-N[42] from resonance assignments. The bar height represents the probability of predicted secondary structures. The S^2 order parameter, a measurement of rigidity, is plotted by the dark lines. The thick color lines at the top highlight segments of secondary structured units, blue for β-strands, red for α-helices, and green for flexible loops.

raphy (cryoET) studies indicate[22] that pentamers in authentic HIV capsids adopt different NTD−NTD and NTD−CTD interfaces from those in cross-linked hexamers and pentamers,[14,21] though details could not be determined at the 8.8 Å resolution. Meanwhile, the limited resolution also prohibits site-specific distinction of the RSV CAs in the pentameric versus the hexameric state.[17,18,20] Analyses of the RSV CA planar hexameric sheets at 4 Å resolution suggest that both NTD−NTD and CTD dimer interfaces are rigid, but the NTD−CTD orientation varies around the NTD−CTD interface. However, no curvature is present in these assemblies.[19]

Recent atomic resolution X-ray diffraction models of native HIV CA hexamer crystals identified prevalent hydrogen bonds (H-bonds) at all interfaces.[23] It was also shown that variation of the hydration level triggers changes of NTD−CTD orientations around the interdomain linker, which was attributed to assembly plasticity. In addition, notable differences were observed at the CTD dimer interface compared with that in isolated hexamers of cross-linked mutant HIV CA,[14,15] with a tighter CTD trimer interface.[16] Solid -state NMR (ssNMR) was also applied to study various HIV CA assemblies.[24−32] Residues at the ends of each domain and in the cyclophilin A binding loop (residues 87−100) were shown to be highly mobile, while the interdomain flexible linker undergoes millisecond motions, which could alter the interdomain orientation and cause assembly polymorphism.[26,28,30,32] However, no major distinctions at the molecular level were identified between CAs in the pentameric and hexameric assemblies.[25]

In our previous work, we obtained the first high-resolution model for the RSV CA tubular assembly by combining ssNMR and cryoelectron microscopy constraints.[33] We showed that the curvature variations in the hexameric lattice are mediated by varying the CA side chain configurations, while their backbone structure remains largely unchanged. In this work, we report the high-resolution structural model of the RSV CA in its $T = 1$ capsid assembly, with 1.97 Å root-mean-square deviation (RMSD) of carbon Cα among CA monomers. Molecular dynamics flexible fitting (MDFF)[32] allows site-specific resolution of the molecular details of CA pentamers by combining secondary structural constraints from our ssNMR results with the previously published cryoET model (EMDB 5773) at 8.5 Å.[17] Importantly, the model unambiguously reveals a simple mechanism for the RSV CA to switch its conformation between the hexameric and pentameric state at both a residue-specific and global level: directed by large torsion angle changes to only about a dozen residues, the subunit undergoes a 33.92 ± 7.28°

https://doi.org/10.1021/acs.jpclett.1c01769
J. Phys. Chem. Lett. 2021, 12, 7768−7776

interdomain rotation via the flexible interdomain linker, with little adjustment of the domain structure or interface contacts. This knowledge provides an invaluable molecular basis at a site-specific level to advance our understanding of the retroviral capsid assembly mechanism.

Wild-type RSV CAs tend to form either tubes or large polymorphic structures comprising mostly hexamers.[34] To prepare an assembly comprising exclusively pentamers, we used the I190V RSV mutant.[35] When solution at 6 mg/mL was mixed with an equal volume of 1 M sodium phosphate buffer at pH 8, predominantly small empty spherical structures were formed. To assess the morphology of the assemblies, negatively stained transmission electron microscopy (TEM) images were recorded. A representative view is shown in Figure 1A. Measurements of the assembly diameter were analyzed, and a histogram is shown in Figure 1B. The average size of the spherical assemblies is about 18.5 nm, consistent with the previously reported value for the $T = 1$ capsid.[18] These data confirm that our assembly sample consists nearly entirely of CA pentamers.

To perform NMR experiments, uniform ^{13}C, ^{15}N labeled CA (U-CA) was expressed. Its assembly produces 2D spectra with excellent resolution. A 2D $^{15}N-^{13}C$ correlation spectrum with cross peaks created by 50 ms mixing of dipolar assisted rotational resonance[36,37] (DARR) is shown in Figure 1C. The typical line width is about 0.7 ppm along the ^{13}C dimension and 1.2 ppm along the ^{15}N dimension, comparable to that of our prior RSV CA tubular assembly under moderate magic angle spinning (MAS)[33] and similar to that of other highly ordered protein structures[38−40] and HIV CA assemblies.[24−32] This indicates that the RSV CA adopts a highly ordered structure at the molecular level, consistent with our TEM evaluation.

To perform sequential assignments, a series of 2D and 3D correlation spectra were recorded with the U-CA, as detailed in Table S1 in the Supporting Information. All congested resonances in 2D spectra can be resolved in the 3D NCaCX and partially resolved in 3D NCOCX spectra. We note that only one set of resonances was identified for each residue, which suggests that the RSV CA adopts a unique and well-defined conformation in the $T = 1$ assembly. 3D CaNCX spectra were also recorded. However, given the weaker signal-to-noise ratio (SNR) and the similarity to assigned chemical shifts in the RSV CA tubular assembly,[33] the benefit of CaNCX was very limited to help the sequential assignments. Manual sequential assignments were performed by a backbone walk to link resonances in 3D NCaCX and NCOCX. Together, 115 residues were sequentially assigned in this manner. Example stretches of the sequential walk assignments between residues 53−65 and residues 101−116 are shown in Figures S1 and S2 in the Supporting Information. Additionally, 104 well-resolved residues were identified in either the 3D NCaCX or NCOCX spectra. Although the backbone walk cannot be achieved for these residues, they exhibit signals nearly identical to those observed in our prior studies of the tubular assembly.[33] These observations provide a high level of certainty regarding their identities.

Resonances in these 3D correlation spectra were acquired by cross-polarization (CP) transfer, mediated by anisotropic dipolar interactions (through space). Thus, only residues in rigid segments in the assembly would contribute. To detect residues in the flexible segments, an INEPT-TOBSY spectrum was acquired by polarization transfer mediated by isotropic J coupling (through bond),[41] shown in Figure S3. Five residues were identified with a narrow line width comparable to solution NMR and chemical shifts close to random coil values. These residues undergo fast motion, as seen in the soluble state. They were assigned to P230, L231, T232, G235, and I236, like those at the tail of the CTD resolved in our prior tubular assembly work.[33] We also note that signals in the INEPT-TOBSY spectrum of our $T = 1$ capsid assembly are much weaker than those of the tubular assembly. It implies that these residues at the CTD tail are probably not as mobile as those in the tubular assembly, leading to an attenuated signal intensity.

Altogether, 224 residues were assigned for the 237-residue RSV CA in its $T = 1$ capsid assembly. The assignments were deposited in the Biological Magnetic Resonance Data Bank (BMRB), with BMRB ID 50550, and are also shown in Table S2. The following residues are missing from both through bond and through space transferred spectra: residues 47, 50, 88, 95, 117, 157, 173, 218, 219, 229, 233, 234, and 237. Except for residue 173 in the middle of helix 9, the missing residues in our $T = 1$ capsid assembly are all in the flexible loop regions between helices. Most likely, this is because their motions are in a range not sensitive to ssNMR detection, with motions too fast for CP transfer but too slow for the J coupling (at tens of microseconds to milliseconds). In contrast, missing residues in the tubular assembly were residues 150, 229, and 230.[33] In addition, we note the average SNR in our $T = 1$ capsid assembly is nearly 2.5 fold weaker than that in the tubular assembly,[33] while the spectral line width and acquisition conditions (experiment setup and the amount of proteins in NMR rotors) are comparable. This suggests that the molecular ordering in the hexameric and pentameric assembly is comparable. The weaker signal intensity in the pentameric assembly is probably due to the shift of the overall protein dynamics toward the microseconds scale, which attenuates the dipolar interactions and renders the CP transfer less effective in our 3D ssNMR experiments.

On the basis of the assignments, the secondary structure composition and local dynamics were derived with TALOS-N,[42] shown in Figure 1D. Except for three residues, predictions for residues without assignments were still considered as "strong" or "generous" by TALOS-N, based on assignments of adjacent residues and the match of the hepta-peptide sequence.[42] In addition, despite the provided assignments, predicted torsion angles of another 27 residues are considered as "WARN" by TALOS-N, marked by light gray bars in Figure S4A. The number of "WARN" prediction is on par with that of our previous tubular assembly work (29 residues, shown in Figure S4B).[33] Moreover, 16 of these residues overlap in two assemblies, while the rest lie adjacent to these mutual "WARN" residues. Except for residue 189 that is next to the mutation site, all these "WARN" predictions are residues in structure-less regions. Such "WARN" predictions are not necessarily incorrect or unreliable, due to the insensitivity of structure-less segments in the X-ray models used by TALOS-N.[42] Thus, the comparison of TALOS-N predictions also corroborates the quality of our assignments of the $T = 1$ capsid sample.

Overall, the RSV CA in the $T = 1$ capsid assembly adopts a conformation nearly identical to that in the tubular assembly,[33] with the exception for a small number of residues. This notable difference can be overviewed by the overlay of the 2D $^{15}N-^{13}C$ correlation spectra, as shown in Figure 1C. Note that some weak resonances not observed in the 2D spectra of the $T = 1$ capsid did show up in our 3D spectra with longer DARR mixing and signal average. A more accurate and quantitative comparison is

https://doi.org/10.1021/acs.jpclett.1c01769
J. Phys. Chem. Lett. 2021, 12, 7768−7776

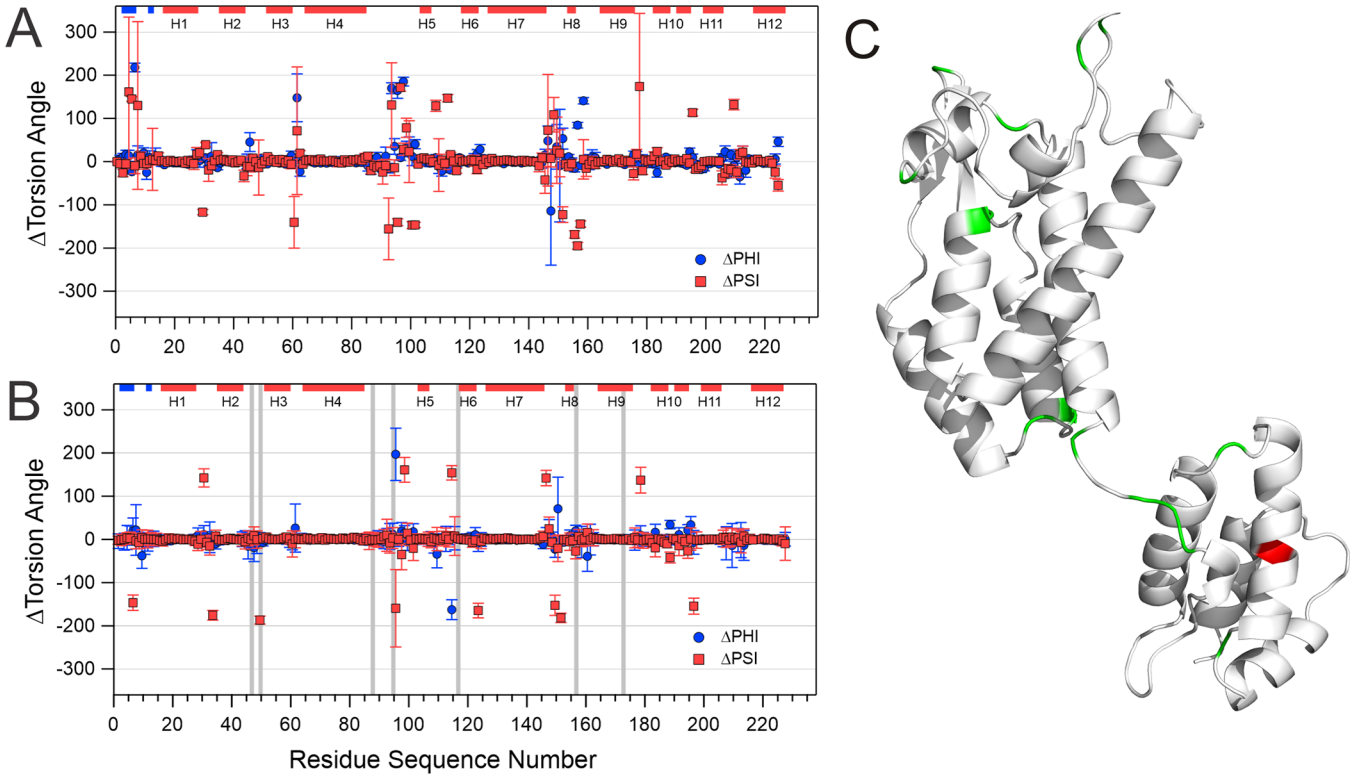

Figure 2. Torsion angle variations of the RSV CA in its $T = 1$ capsid and tubular assembly. (A) and (B) are the torsion angle differences computed *in silico* from the $T = 1$ capsid and prior tubular assembly models[32] and derived by TALOS-N[42] from NMR assignments, respectively. The thick color lines at the top highlight segments of secondary structured units, blue for β-strands and red for α-helices. The gray bars in (B) mark those lacking assignments, but their torsion angles were still predicted by TALOS-N based on assignments of adjacent residues and the match of the hepta-sequence. (C) Residues with NMR-derived torsion angle differences ≥100° between two assemblies colored in green on a subunit from the $T = 1$ capsid model. The I190V mutation is marked by red.

presented in Figure S4: the secondary chemical shifts[43] of the $T = 1$ capsid and the tubular assembly[33] are shown in Figure S4A,B, with their differences plotted in Figure S4C, where only 18 residues exhibit changes of secondary shifts ≥2.5 ppm. Residues with changes of ^{13}C or ^{15}N resonances greater than 2.0 ppm are also labeled in Figure 1C for clarity. This is in clear contrast to the comparison of tubular assemblies with a 2-fold change of diameters (average diameter ∼60 nm vs 130 nm), which showed nearly identical Cα resonances for all residues, with shifted signals associated with side chains.[33] This indicates that CAs have to reconfigure both their backbones and side chains to adapt to the curvature associated with the pentameric assembly, while curvature changes in the pure hexameric lattice can be accommodated by side chain rearrangements alone.

To obtain the structural model for the RSV CA $T = 1$ capsid, data-guided simulations[32] were performed to combine our ssNMR constraints with the 8.5 Å cryoET density (accession code EMDB 5773),[17] with protocols described in the Supporting Information. The simulated model described 60 CA monomers, arranged in a $T = 1$ icosahedron, solvated with TIP3P water,[44] and ionized to a salt concentration of 500 mM NaCl (Figure S5A,B). Figure S5C shows RSV CA monomers extracted from a system of the solvated $T = 1$ capsid simulation and aligned by the backbone atoms, with 1.97 Å RMSD of Cα among CA monomers. This alignment shows the highly uniform structure of subunits in the $T = 1$ capsid, similar to those in the tubular model. Therefore, our model allows analyses to pinpoint the distinct RSV CA conformation at a site-specific resolution in different assemblies.

Next, we computed the torsion angles of the RSV CAs measured directly from the *in silico* tubular and the 60 CA monomers in the $T = 1$ capsid assembly models. Their differences are plotted in Figure 2A. The results agree well with those predicted by TALOS-N[42] derived directly from NMR chemical shifts (Figure 2B), which confirms the quality of our assignments and the model obtained by the integrative approach.[32] The larger error bars in the flexible segments derived from the *in silico* models are as expected. They are computed as the standard deviations of the 60 CA monomers, as explained in the Supporting Information. The conformations of these flexible loops fluctuate from monomer to monomer over the short time femtoseconds scale of MD simulations but exhibit a more uniform average over the much longer tens of milliseconds time scale by ssNMR. Consistently, the regions in the RSV CA with the largest torsion angle differences are located in the β-hairpin around residues 1−16, the flexible loop and flexible interdomain linker regions encompassing residues 87−100 and 145−156, respectively. In particular, torsion angle differences based on our NMR assignments pinpoint a dozen residues with torsion angle differences greater than 100°. Their assignments in the 3D NCaCX spectra are plotted in Figure S6. They reveal the site-specific changes that the RSV CA must undergo to switch its conformation from a quasi-equivalent hexameric to a pentameric state to induce acute curvature in assemblies.

Shown in Figure 3, our $T = 1$ assembly model also resolves the four intermolecular CA interfaces, critical for capsid stability and morphology. As shown in Figure 3B−E, close inspection

https://doi.org/10.1021/acs.jpclett.1c01769
J. Phys. Chem. Lett. 2021, 12, 7768−7776

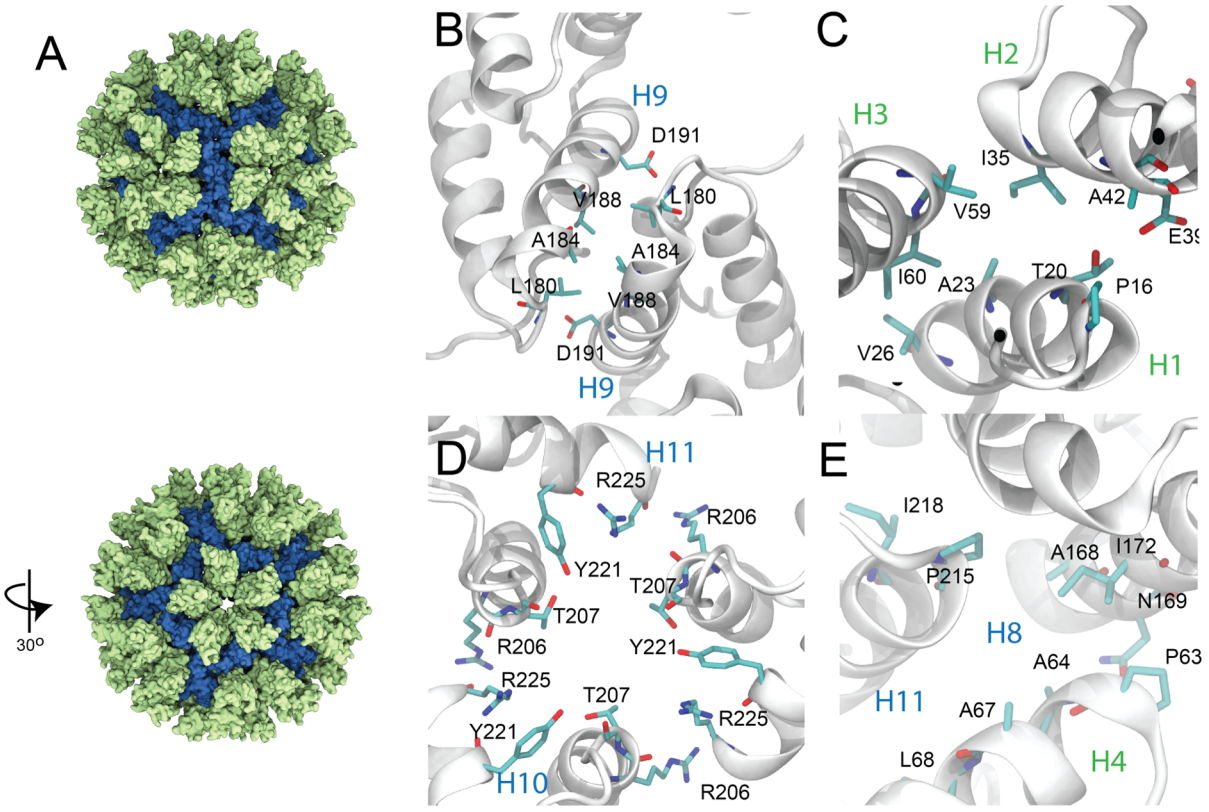

Figure 3. Four intermolecular assembly interfaces in the $T = 1$ capsid model. (A) At the residue-specific level. (B) The dimeric interface is between helix 9 of adjacent subunits. (C) The NTD−NTD interface comprises helices 1 to 3 of each subunit in the pentamer. (D) The CTD trimeric interface involves helices 11 and 10. (E) The NTD−CTD interface is between helices 4, 8, and 11.

confirms that the same set of residues are employed to stabilize each interface in both pentamers in the RSV CA $T = 1$ capsid assembly and hexamers in the tubular assembly.[33] Interestingly, torsion angle analysis shows that differences in backbone dihedral angles of these interfacial residues are limited compared to other regions of CA, such as residues of the flexible interdomain linker and other flexible regions. In the NTD, residues Leu61 and Gly62 situated near the H1−H2−H3 bundle show notable torsion angle differences, although they are positioned away from the helical bundle interior (Figure 3C). Residues comprising the NTD−CTD interface (Figure 3E) show consistent torsion angles, while Ser178—downstream of H8 and the residues which interface with H4 and H11—shows a dramatic change of the psi dihedral angle. Ser178 precedes the dimeric interface in CA, which, like other interfaces, does not demonstrate large torsion angle differences among assembly models. This observation follows the trend of torsion angle differences concentrated among residues preceding and succeeding structured interfaces. Continuing down the CA sequence and preceding the trimer interface is Lys196, which additionally substantiates our observation as to where torsion angles differ in distinct CA assemblies. In summary, the molecular differences in torsion angles do not cause large variations of assembly interfaces in the CA pentameric assembly compared to its hexameric assembly. It shows the remarkable efficiency of the viral CA to achieve assembly versatility with minimum structural modulation.

Thus, our above analyses show that only subtle differences exist in the RSV CA folding at the molecular level, in hexameric versus pentameric assemblies. Then, the question arises: How do such subtle conformational differences translate into one less subunit in the quasi-equivalent assemblies? To answer this, we first aligned the monomers extracted from the RSV tubular and $T = 1$ capsid assembly by their backbone atoms in the NTD, as shown in Figure 4A. Then, principal component analysis (PCA) was applied to identify the dynamical modes or essential components that set apart the molecular folding in the hexameric versus pentameric assembly, with their contribution ranked by the overall variance of the data set.

Interestingly, our PCA reveals a dominant mode that shifts an RSV CA monomer in the hexameric tubular assembly to that in the $T = 1$ capsid assembly, contributing to more than half of all the variance in the data set. As shown in Figures 4B,C, this mode corresponds to a 33.92° ± 7.28° rotation and 5.94 ± 1.04 Å center-of-mass translation of the CTD mediated by residues in the flexible linker, encompassing residues 147−149, as well as residues 151−156 in the 3_{10} helix. In fact, nearly the entire structural rearrangements of the CTD can be captured by the top three PCs, as shown in Figure 4D. An animation of the top three PCs is shown in the movie in the Supporting Information. The animation also shows that the additional structural changes in the flexible loop and β-hairpin region are concomitant with the structural rearrangements of the CTD.

Previously, ssNMR were applied to study HIV CA assemblies of tubular, spherical, and conical assemblies. No major chemical shift differences of backbone atoms were found to correlate with assembly morphologies.[25,31] It agrees with our prior work assessments that the backbone conformations of the RSV CA are nearly the same in tubes of different diameters[33] but contrasts with our ssNMR results that unambiguously correlate the residues in different conformations in $T = 1$ capsid and tubular assemblies. This difference is probably due to the low

https://doi.org/10.1021/acs.jpclett.1c01769
J. Phys. Chem. Lett. 2021, 12, 7768−7776

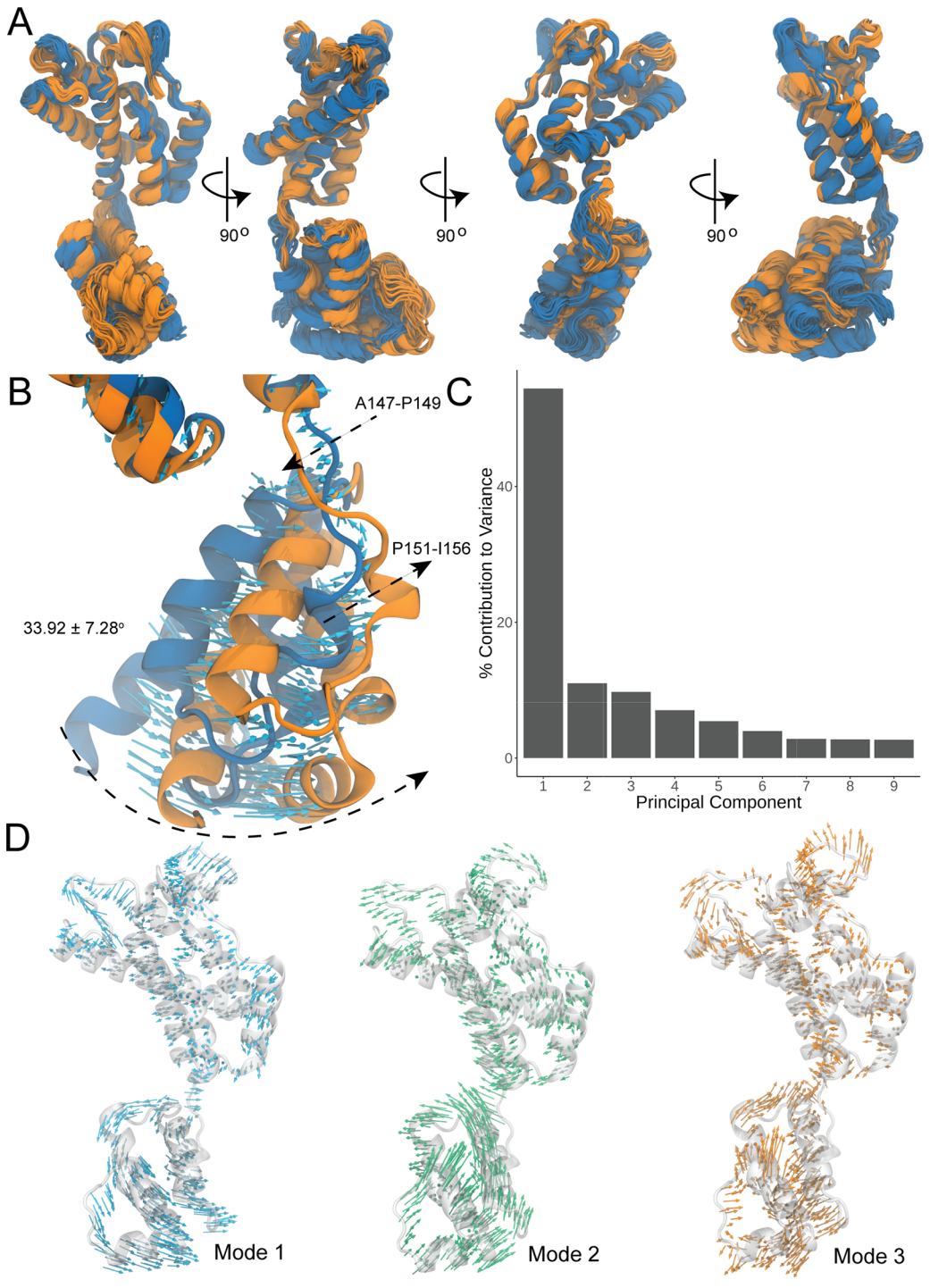

Figure 4. Differences of the RSV CA in quasi-equivalent assemblies revealed by PCA. (A) 360° view of a CA monomer from the $T = 1$ capsid (orange) aligned by its NTD against that from the tubular (blue) assembly. (B) PCs reveal a rotation plus translation motion around the flexible interdomain linker to transform a CA in its pentameric assembly to that in the hexameric assembly. The blue vectors denote the direction and magnitude of the motion. (C) The contribution of each PC to the overall variance of the data set. (D) Visualizations of the first three PCs, as porcupine plots—each residue specific motion is shown as a colored vector. For each graphical depiction, the magnitudes of the PCs are normalized.

concentration of pentamers in those large, polymorphic HIV conical and spherical assemblies, which masks their structural signatures in the overwhelmingly hexameric subunits. In contrast, our sample comprises nearly exclusively the uniform pentameric assemblies (Figure 1B). Hence, the observed sharp chemical shift differences in this work by ssNMR testify to its unique strength to detect even the subtle differences at a site-specific resolution, between quasi-equivalent pentameric and hexameric assemblies, which is challenging to obtain otherwise. Combined with MDFF,[32] the ssNMR restraints are critical to refine the 8.5 Å resolution cryoET density map to the high-resolution model reported in this work. Our PCA results corroborate our ssNMR observation and further revealed how these key residues in the RSV CA orchestrate the structural transformation to form a pentamer or hexamer, without major modulations of the assembly interfaces or the structures of NTD

https://doi.org/10.1021/acs.jpclett.1c01769
J. Phys. Chem. Lett. 2021, 12, 7768−7776

and CTD. Moreover, as shown in Figure S7, this structural transformation leads to a NTD−CTD orientation in the pentamer that matches what was identified by cryoET in the authentic HIV virion, where the host factors cleavage and polyadenylation specificity factor 6 (CPSF6) binding pocket in the NTD of the neighboring subunit is more exposed than that in the NTD of a monomer in the hexamer.[22] It suggests that a common structural transition of the subunit CA is employed to switch between the pentameric and hexameric assembly for both HIV and RSV CAs. Another interesting question is, how different are the necessary structural transitions for two different kinds of curvature inductions: from the flat hexameric lattice to tube and to the pentameric assembly? For this purpose, we aligned the monomeric CA in our RSV CA tubular and $T = 1$ capsid assemblies, against that in the flat RSV CA hexameric sheet (3TIR.pdb).[19] As shown in Figure S8, they require conformational rearrangements with comparable amplitudes, with 3.868 and 4.067 Å RMSD, respectively, although both the numerical values and visual inspection confirm that the changes associated with the shift to a pentameric assembly are slightly greater. It agrees with our observations that shifted NMR resonances are present in both backbone and side chain regions when comparing the tubular and $T = 1$ capsid assembly, while only side chain resonances are different comparing tubes of different diameters.[33] Hence, our results provide critical new insights to unraveling the mystery of how retroviruses control the curvature in their capsid assemblies.

As listed in Figure S6, and shown in Figure 2B,C, all the residues exhibiting large changes of torsion angles are isolated individuals and sparsely positioned in the flexible loops connecting neighboring structured helices, or in the flexible interdomain linker. It seems that they work like the hinge of a door, to activate the necessary rearrangements of structured segments in a CA monomer to shift between the quasi-equivalent pentameric and hexameric state. Moreover, the changes of NMR resonances (Figure S4C) reveal that frequently residues around these isolated points also manifest appreciable or significant changes of chemical shifts, especially around the flexible interdomain linker and I190V mutation point. Therefore, our NMR data further indicate that such critical and sparsely spaced single point restructures are achieved not just by these isolated residues alone but result from a cohesive and collaborative work of the neighboring residues. In fact, the function of the flexible interdomain linker revealed by our work was hypothesized years ago by both Pornillos et al.[21] and Worthylake et al.[45] Brun et al.[46] and Wacharapornin et al.[47] first demonstrated the detrimental effect of the S149A mutation on HIV viral infectivity. Subsequently, Jiang et al. performed a systematic site-directed mutagenesis study of the HIV CA flexible linker (residues 145−151).[8] Their results showed that residues in the nonstructured interdomain linker regions are critical for the correct assembly and stability of HIV capsid and that specific mutations attenuate or completely abolish infectivity.[8] Furthermore, recent ssNMR work found that the flexible interdomain linker in the HIV CA tubular assemblies adopts four distinct conformations,[28] undergoing millisecond scale dynamics.[26,28,30,32] which would allow such a modulation to take place. Our results support these reports and further correlate the detailed molecular level motions of the flexible linker with the curvature control.

Nevertheless, it is not yet clear how this motion of the flexible interdomain linker is triggered and regulated in the authentic viral particle assembly. Solution NMR studies by Deshmukh et al. defined the conformation space of interdomain orientation sampled by HIV CA dimers in low salt solution and suggested that the selection of the pentameric over hexameric assembly is tightly regulated by such motion.[3] Accounting for the conformation space defined by solution NMR, coarse-grained simulations by Qiao et al. also showed that the HIV CA pentamers can be readily incorporated into a hexameric lattice at concentrations comparable to experimental conditions, and it requires a highly specific NTD to CTD orientation but not sensitive to particular structural variations within individual domains.[48] Subsequent coarse-gained simulations by Grime et al. suggest that a higher concentration favors the assembly of an HIV CA pentamer over a hexamer.[49] Thus, a possible mechanism for different retroviruses to control their preferred assembly morphology would be to position the locations of such factors that promote the specific torsion angles of the interdomain linker suitable for the pentameric CA assembly. Slight randomization of their locations would displace the locations of resulting pentamers and give rise to the apparent assembly polymorphism.

■ ASSOCIATED CONTENT

Supporting Information

The Supporting Information is available free of charge at https://pubs.acs.org/doi/10.1021/acs.jpclett.1c01769.

Materials and methods, transmission electron microscopy, solid-state NMR experimental setup, protocols for simulation and modeling setup (PDF)

Animation movie showing the structural transformation of a monomeric subunit in the tubular assembly to that in the $T = 1$ capsid (AVI)

■ AUTHOR INFORMATION

Corresponding Authors

Bo Chen − *Department of Physics, University of Central Florida, Orlando, Florida 32816, United States;* orcid.org/0000-0001-5589-2075; Email: Bo.Chen@ucf.edu

Juan R. Perilla − *Department of Chemistry and Biochemistry, University of Delaware, Newark, Delaware 19716, United States;* orcid.org/0000-0003-1171-6816; Email: jperilla@udel.edu

Authors

Tyrone Thames − *Department of Physics, University of Central Florida, Orlando, Florida 32816, United States*

Alexander J. Bryer − *Department of Chemistry and Biochemistry, University of Delaware, Newark, Delaware 19716, United States*

Xin Qiao − *Department of Physics, University of Central Florida, Orlando, Florida 32816, United States*

Jaekyun Jeon − *Laboratory of Chemical Physics, National Institute of Diabetes and Digestive and Kidney Diseases (NIDDK), National Institutes of Health, Bethesda, Maryland 20892, United States*

Ryan Weed − *Department of Chemistry, University of Central Florida, Orlando, Florida 32816, United States*

Kaylie Janicki − *Department of Chemistry, University of Central Florida, Orlando, Florida 32816, United States*

Bingwen Hu − *State Key Laboratory of Precision Spectroscopy, Shanghai Key Laboratory of Magnetic Resonance, Institute of Functional Materials, School of Physics and Materials Science,*

https://doi.org/10.1021/acs.jpclett.1c01769
J. Phys. Chem. Lett. 2021, 12, 7768−7776

East China Normal University, Shanghai 200062, PR China; orcid.org/0000-0003-0694-0178

Peter L. Gor'kov − *National High Magnetic Field Laboratory, Florida State University, Tallahassee, Florida 32310, United States*

Ivan Hung − *National High Magnetic Field Laboratory, Florida State University, Tallahassee, Florida 32310, United States;* orcid.org/0000-0001-8916-739X

Zhehong Gan − *National High Magnetic Field Laboratory, Florida State University, Tallahassee, Florida 32310, United States;* orcid.org/0000-0002-9855-5113

Complete contact information is available at: https://pubs.acs.org/10.1021/acs.jpclett.1c01769

Author Contributions

#T.T., A.J.B., and X.Q. contributed equally to this work. B.C. designed the experiments. J.J. identified the initial assembly condition. X.Q. made all the samples. B.C., X.Q., P.L.G., I.H., and Z.G. acquired NMR spectra. X.Q. and B.C. processed and analyzed the spectra. X.Q., T.T., R.W., K.J., B.H., and B.C. made the assignments. A.J.B. and J.R.P. performed simulations and modeling. T.T., A.J.B., J.R.P., and B.C. analyzed the results and prepared the manuscript.

Notes

The authors declare no competing financial interest.

■ ACKNOWLEDGMENTS

The authors acknowledge the gift of the CA plasmid from Prof. Rebecca C. Craven at Pennsylvania State University and consultation on protein purification and assembly, Woonghee Lee at University of Colorado for his help with the program NMRSparky, and Frank Shewmaker at Uniform Services University for molecular weight confirmation with mass spectrometry. We are also obliged to Judith G. Levin for her insightful comments to revise the manuscript. This work was supported by the Midcareer refreshment program of University of Central Florida (B.C.), and the National High Magnetic Field Laboratory through NSF/DMR-1157490, and the State of Florida (P.L.G.; I.H.; ZH.G.) It was also supported by the U.S. National Institutes of Health Grants P50AI1504817 (J.R.P.), P20GM104316 (J.R.P.), and R56AI076121 (J.R.P.). This study used the Extreme Science and Engineering Discovery Environment, which is supported by the National Science Foundation (Grant ACI-1548562) (J.R.P.) and also used XSEDE Bridges and Stampede2 at the Pittsburgh Super Computing Center and Texas Advanced Computing Center, respectively, through allocation MCB170096 (J.R.P.).

■ REFERENCES

(1) Novikova, M.; Zhang, Y. L.; Freed, E. O.; Peng, K. Multiple Roles of HIV-1 Capsid during the Virus Replication Cycle. *Virol. Sin.* **2019**, *34* (2), 119−134.

(2) Vogt, V. Retroviral virions and genomes. In *Retroviruses*; Coffin, J. M., Hughes, S. H., Varmus, H. E., Eds.; Cold Spring Harbor Press: New York, 1997; pp 22−70.

(3) Deshmukh, L.; Schwieters, C. D.; Grishaev, A.; Ghirlando, R.; Baber, J. L.; Clore, G. M. Structure and Dynamics of Full-Length HIV-1 Capsid Protein in Solution. *J. Am. Chem. Soc.* **2013**, *135* (43), 16133−16147.

(4) Gamble, T. R.; Vajdos, F. F.; Yoo, S. H.; Worthylake, D. K.; Houseweart, M.; Sundquist, W. I.; Hill, C. P. Crystal structure of human cyclophilin A bound to the amino-terminal domain of HIV-1 capsid. *Cell* **1996**, *87* (7), 1285−1294.

(5) Gitti, R. K.; Lee, B. M.; Walker, J.; Summers, M. F.; Yoo, S.; Sundquist, W. I. Structure of the amino-terminal core domain of the HIV-1 capsid protein. *Science* **1996**, *273* (5272), 231−235.

(6) Gamble, T. R.; Yoo, S. H.; Vajdos, F. F.; vonSchwedler, U. K.; Worthylake, D. K.; Wang, H.; McCutcheon, J. P.; Sundquist, W. I.; Hill, C. P. Structure of the carboxyl-terminal dimerization domain of the HIV-1 capsid protein. *Science* **1997**, *278* (5339), 849−853.

(7) Ganser-Pornillos, B. K.; von Schwedler, U. K.; Stray, K. M.; Aiken, C.; Sundquist, W. I. Assembly properties of the human immunodeficiency virus type 1 CA protein. *J. Virol.* **2004**, *78* (5), 2545−2552.

(8) Jiang, J. Y.; Ablan, S. D.; Derebail, S.; Hercik, K.; Soheilian, F.; Thomas, J. A.; Tang, S. X.; Hewlett, I.; Nagashima, K.; Gorelick, R. J.; Freed, E. O.; Levin, J. G. The interdomain linker region of HIV-1 capsid protein is a critical determinant of proper core assembly and stability. *Virology* **2011**, *421* (2), 253−265.

(9) Carnes, S. K.; Sheehan, J. H.; Aiken, C. Inhibitors of the HIV-1 capsid, a target of opportunity. *Curr. Opin. HIV AIDS* **2018**, *13* (4), 359−365.

(10) Link, J. O.; Rhee, M. S.; Tse, W. C.; Zheng, J.; Somoza, J. R.; Rowe, W.; Begley, R.; Chiu, A.; Mulato, A.; Hansen, D.; Singer, E.; Tsai, L. K.; Bam, R. A.; Chou, C. H.; Canales, E.; Brizgys, G.; Zhang, J. R.; Li, J. Y.; Graupe, M.; Morganelli, P.; Liu, Q.; Wu, Q. Y.; Halcomb, R. L.; Saito, R. D.; Schroeder, S. D.; Lazerwith, S. E.; Bondy, S.; Jin, D. B.; Hung, M.; Novikov, N.; Liu, X. H.; Villasenor, A. G.; Cannizzaro, C. E.; Hu, E. Y.; Anderson, R. L.; Appleby, T. C.; Lu, B.; Mwangi, J.; Liclican, A.; Niedziela-Majka, A.; Papalia, G. A.; Wong, M. H.; Leavitt, S. A.; Xu, Y. L.; Koditek, D.; Stepan, G. J.; Yu, H.; Pagratis, N.; Clancy, S.; Ahmadyar, S.; Cai, T. Z.; Sellers, S.; Wolckenhauer, S. A.; Ling, J.; Callebaut, C.; Margot, N.; Ram, R. R.; Liu, Y. P.; Hyland, R.; Sinclair, G. I.; Ruane, P. J.; Crofoot, G. E.; McDonald, C. K.; Brainard, D. M.; Lad, L.; Swaminathan, S.; Sundquist, W. I.; Sakowicz, R.; Chester, A. E.; Lee, W. E.; Daar, E. S.; Yant, S. R.; Cihlar, T. Clinical targeting of HIV capsid protein with a long-acting small molecule. *Nature* **2020**, *584* (7822), 614−618.

(11) Yeager, M. Design of in Vitro Symmetric Complexes and Analysis by Hybrid Methods Reveal Mechanisms of HIV Capsid Assembly. *J. Mol. Biol.* **2011**, *410* (4), 534−552.

(12) Ganser, B. K.; Li, S.; Klishko, V. Y.; Finch, J. T.; Sundquist, W. I. Assembly and analysis of conical models for the HIV-1 core. *Science* **1999**, *283* (5398), 80−83.

(13) Ganser-Pornillos, B. K.; Cheng, A.; Yeager, M. Structure of full-length HIV-1CA: a model for the mature capsid lattice. *Cell* **2007**, *131* (1), 70−79.

(14) Pornillos, O.; Ganser-Pornillos, B. K.; Kelly, B. N.; Hua, Y. Z.; Whitby, F. G.; Stout, C. D.; Sundquist, W. I.; Hill, C. P.; Yeager, M. X-Ray Structures of the Hexameric Building Block of the HIV Capsid. *Cell* **2009**, *137* (7), 1282−1292.

(15) Pornillos, O.; Ganser-Pornillos, B. K.; Banumathi, S.; Hua, Y. Z.; Yeager, M. Disulfide Bond Stabilization of the Hexameric Capsomer of Human Immunodeficiency Virus. *J. Mol. Biol.* **2010**, *401* (5), 985−995.

(16) Zhao, G. P.; Perilla, J. R.; Yufenyuy, E. L.; Meng, X.; Chen, B.; Ning, J. Y.; Ahn, J.; Gronenborn, A. M.; Schulten, K.; Aiken, C.; Zhang, P. J. Mature HIV-1 capsid structure by cryo-electron microscopy and all-atom molecular dynamics. *Nature* **2013**, *497* (7451), 643−646.

(17) Keller, P. W.; Huang, R. K.; England, M. R.; Waki, K.; Cheng, N. Q.; Heymann, J. B.; Craven, R. C.; Freed, E. O.; Steven, A. C. A Two-Pronged Structural Analysis of Retroviral Maturation Indicates that Core Formation Proceeds by a Disassembly-Reassembly Pathway Rather than a Displacive Transition. *J. Virol.* **2013**, *87* (24), 13655−13664.

(18) Cardone, G.; Purdy, J. G.; Cheng, N. Q.; Craven, R. C.; Steven, A. C. Visualization of a missing link in retrovirus capsid assembly. *Nature* **2009**, *457* (7230), 694−699.

(19) Bailey, G. D.; Hyun, J. K.; Mitra, A. K.; Kingston, R. L. A Structural Model for the Generation of Continuous Curvature on the Surface of a Retroviral Capsid. *J. Mol. Biol.* **2012**, *417* (3), 212−223.

(20) Hyun, J. K.; Radjainia, M.; Kingston, R. L.; Mitra, A. K. Proton-driven Assembly of the Rous Sarcoma Virus Capsid Protein Results in

the Formation of Icosahedral Particles. *J. Biol. Chem.* **2010**, *285* (20), 15056−15064.
(21) Pornillos, O.; Ganser-Pornillos, B. K.; Yeager, M. Atomic-level modelling of the HIV capsid. *Nature* **2011**, *469* (7330), 424−427.
(22) Mattei, S.; Glass, B.; Hagen, W. J. H.; Krausslich, H. G.; Briggs, J. A. G. The structure and flexibility of conical HIV-1 capsids determined within intact virions. *Science* **2016**, *354* (6318), 1434−1437.
(23) Gres, A. T.; Kirby, K. A.; KewalRamani, V. N.; Tanner, J. J.; Pornillos, O.; Sarafianos, S. G. X-ray crystal structures of native HIV-1 capsid protein reveal conformational variability. *Science* **2015**, *349* (6243), 99−103.
(24) Chen, B.; Tycko, R. Structural and dynamical characterization of tubular HIV-1 capsid protein assemblies by solid state nuclear magnetic resonance and electron microscopy. *Protein Sci.* **2010**, *19* (4), 716−730.
(25) Lu, J. X.; Bayro, M. J.; Tycko, R. Major Variations in HIV-1 Capsid Assembly Morphologies Involve Minor Variations in Molecular Structures of Structurally Ordered Protein Segments. *J. Biol. Chem.* **2016**, *291* (25), 13098−13112.
(26) Zhang, H. L.; Hou, G. J.; Lu, M. M.; Ahn, J.; Byeon, I. J. L.; Langmead, C. J.; Perilla, J. R.; Hung, I.; Gor'kov, P. L.; Gan, Z. H.; Brey, W. W.; Case, D. A.; Schulten, K.; Gronenborn, A. M.; Polenova, T. HIV-1 Capsid Function Is Regulated by Dynamics: Quantitative. Atomic-Resolution Insights by Integrating Magic-Angle-Spinning NMR, QM/MM, and MD. *J. Am. Chem. Soc.* **2016**, *138* (42), 14066−14075.
(27) Liu, C.; Perilla, J. R.; Ning, J. Y.; Lu, M. M.; Hou, G. J.; Ramalho, R.; Himes, B. A.; Zhao, G. P.; Bedwell, G. J.; Byeon, I. J.; Ahn, J.; Gronenborn, A. M.; Prevelige, P. E.; Rousso, I.; Aiken, C.; Polenova, T.; Schulten, K.; Zhang, P. J. Cyclophilin A stabilizes the HIV-1 capsid through a novel non-canonical binding site. *Nat. Commun.* **2016**, *7*, 10714.
(28) Lu, M. M.; Russell, R. W.; Bryer, A. J.; Quinn, C. M.; Hou, G. J.; Zhang, H. L.; Schwieters, C. D.; Perilla, J. R.; Gronenborn, A. M.; Polenova, T. Atomic-resolution structure of HIV-1 capsid tubes by magic-angle spinning NMR. *Nat. Struct. Mol. Biol.* **2020**, *27* (9), 863−869.
(29) Bayro, M. J.; Chen, B.; Yau, W. M.; Tycko, R. Site-Specific Structural Variations Accompanying Tubular Assembly of the HIV-1 Capsid Protein. *J. Mol. Biol.* **2014**, *426* (5), 1109−1127.
(30) Byeon, I. J. L.; Hou, G. J.; Han, Y.; Suiter, C. L.; Ahn, J.; Jung, J.; Byeon, C. H.; Gronenborn, A. M.; Polenova, T. Motions on the Millisecond Time Scale and Multiple Conformations of HIV-1 Capsid Protein: Implications for Structural Polymorphism of CA Assemblies. *J. Am. Chem. Soc.* **2012**, *134* (14), 6455−6466.
(31) Han, Y.; Ahn, J.; Concel, J.; Byeon, I. J. L.; Gronenborn, A. M.; Yang, J.; Polenova, T. Solid-State NMR Studies of HIV-1 Capsid Protein Assemblies. *J. Am. Chem. Soc.* **2010**, *132* (6), 1976−1987.
(32) Perilla, J. R.; Hadden-Perilla, J. A.; Gronenborn, A. M.; Polenova, T. Integrative structural biology of HIV-1 capsid protein assemblies: combining experiment and computation. *Curr. Opin. Virol.* **2021**, *48*, 57−64.
(33) Jeon, J.; Qiao, X.; Hung, I.; Mitra, A. K.; Desfosses, A.; Huang, D.; Gor'kov, P. L.; Craven, R. C.; Kingston, R. L.; Gan, Z. H.; Zhu, F. Q.; Chen, B. Structural Model of the Tubular Assembly of the Rous Sarcoma Virus Capsid Protein. *J. Am. Chem. Soc.* **2017**, *139* (5), 2006−2013.
(34) Purdy, J. G.; Flanagan, J. M.; Ropson, I. J.; Craven, R. C. Retroviral Capsid Assembly: A Role for the CA Dimer in Initiation. *J. Mol. Biol.* **2009**, *389* (2), 438−451.
(35) Bowzard, J. B.; Wills, J. W.; Craven, R. C. Second-site suppressors of Rous sarcoma virus CA mutations: Evidence for interdomain interactions. *J. Virol.* **2001**, *75* (15), 6850−6856.
(36) Takegoshi, K.; Nakamura, S.; Terao, T. C-13-H-1 dipolar-assisted rotational resonance in magic-angle spinning NMR. *Chem. Phys. Lett.* **2001**, *344* (5−6), 631−637.
(37) Morcombe, C. R.; Gaponenko, V.; Byrd, R. A.; Zilm, K. W. Diluting abundant spins by isotope edited radio frequency field assisted diffusion. *J. Am. Chem. Soc.* **2004**, *126* (23), 7196−7197.
(38) Lu, J. X.; Qiang, W.; Yau, W. M.; Schwieters, C. D.; Meredith, S. C.; Tycko, R. Molecular Structure of beta-Amyloid Fibrils in Alzheimer's Disease Brain Tissue. *Cell* **2013**, *154* (6), 1257−1268.
(39) Tuttle, M. D.; Comellas, G.; Nieuwkoop, A. J.; Covell, D. J.; Berthold, D. A.; Kloepper, K. D.; Courtney, J. M.; Kim, J. K.; Barclay, A. M.; Kendall, A.; Wan, W.; Stubbs, G.; Schwieters, C. D.; Lee, V. M. Y.; George, J. M.; Rienstra, C. M. Solid-state NMR structure of a pathogenic fibril of full-length human alpha-synuclein. *Nat. Struct. Mol. Biol.* **2016**, *23* (5), 409−415.
(40) Van Melckebeke, H.; Wasmer, C.; Lange, A.; Ab, E.; Loquet, A.; Bockmann, A.; Meier, B. H. Atomic-Resolution Three-Dimensional Structure of HET-s(218−289) Amyloid Fibrils by Solid-State NMR Spectroscopy. *J. Am. Chem. Soc.* **2010**, *132* (39), 13765−13775.
(41) Hardy, E. H.; Verel, R.; Meier, B. H. Fast MAS total through-bond correlation spectroscopy. *J. Magn. Reson.* **2001**, *148* (2), 459−464.
(42) Shen, Y.; Bax, A. Protein backbone and sidechain torsion angles predicted from NMR chemical shifts using artificial neural networks. *J. Biomol. NMR* **2013**, *56* (3), 227−241.
(43) Luca, S.; Filippov, D. V.; van Boom, J. H.; Oschkinat, H.; de Groot, H. J. M.; Baldus, M. Secondary chemical shifts in immobilized peptides and proteins: A qualitative basis for structure refinement under Magic Angle Spinning. *J. Biomol. NMR* **2001**, *20* (4), 325−331.
(44) Jorgensen, W. L.; Chandrasekhar, J.; Madura, J. D.; Impey, R. W.; Klein, M. L. Comparison of Simple Potential Functions for Simulating Liquid Water. *J. Chem. Phys.* **1983**, *79* (2), 926−935.
(45) Worthylake, D. K.; Wang, H.; Yoo, S. H.; Sundquist, W. I.; Hill, C. P. Structures of the HIV-1 capsid protein dimerization domain at 2.6 angstrom resolution. *Acta Crystallographica Section D-Structural. Acta Crystallogr., Sect. D: Biol. Crystallogr.* **1999**, *55*, 85−92.
(46) Brun, S.; Solignat, M.; Gay, B.; Bernard, E.; Chaloin, L.; Fenard, D.; Devaux, C.; Chazal, N.; Briant, L. VSV-G pseudotyping rescues HIV-1CA mutations that impair core assembly or stability. *Retrovirology* **2008**, *5*, 57.
(47) Wacharapornin, P.; Lauhakirti, D.; Auewarakul, P. The effect of capsid mutations on HIV-1 uncoating. *Virology* **2007**, *358* (1), 48−54.
(48) Qiao, X.; Jeon, J.; Weber, J.; Zhu, F.; Chen, B. Mechanism of polymorphism and curvature of HIV capsid assemblies probed by 3D simulations with a novel coarse grain model. *Biochim. Biophys. Acta, Gen. Subj.* **2015**, *1850* (11), 2353−2367.
(49) Grime, J. M. A.; Dama, J. F.; Ganser-Pornillos, B. K.; Woodward, C. L.; Jensen, G. J.; Yeager, M.; Voth, G. A. Coarse-grained simulation reveals key features of HIV-1 capsid self-assembly. *Nat. Commun.* **2016**, *7*, 11568.

https://doi.org/10.1021/acs.jpclett.1c01769
J. Phys. Chem. Lett. 2021, 12, 7768−7776